biophysica

MDPI

Article

Elucidating the Influence of Lipid Composition on Bilayer Perturbations Induced by the N-Terminal Region of the Huntingtin Protein

Yasith Indigahawela Gamage and Jianjun Pan *

Department of Physics, University of South Florida, Tampa, FL 33620, USA; yasith@usf.edu
* Correspondence: panj@usf.edu

Abstract: Understanding the membrane interactions of the N-terminal 17 residues of the huntingtin protein (HttN) is essential for unraveling its role in cellular processes and its impact on huntingtin misfolding. In this study, we used atomic force microscopy (AFM) to examine the effects of lipid specificity in mediating bilayer perturbations induced by HttN. Across various lipid environments, the peptide consistently induced bilayer disruptions in the form of holes. Notably, our results unveiled that cholesterol enhanced bilayer perturbation induced by HttN, while phosphatidylethanolamine (PE) lipids suppressed hole formation. Furthermore, anionic phosphatidylglycerol (PG) and cardiolipin lipids, along with cholesterol at high concentrations, promoted the formation of double-bilayer patches. This unique structure suggests that the synergy among HttN, anionic lipids, and cholesterol can enhance bilayer fusion, potentially by facilitating lipid intermixing between adjacent bilayers. Additionally, our AFM-based force spectroscopy revealed that HttN enhanced the mechanical stability of lipid bilayers, as evidenced by an elevated bilayer puncture force. These findings illuminate the complex interplay between HttN and lipid membranes and provide useful insights into the role of lipid composition in modulating membrane interactions with the huntingtin protein.

Keywords: atomic force microscopy; force spectroscopy; lipid bilayer structure; membrane fusion; lipid specificity; anionic lipids; cardiolipin

Citation: Gamage, Y.I.; Pan, J. Elucidating the Influence of Lipid Composition on Bilayer Perturbations Induced by the N-Terminal Region of the Huntingtin Protein. *Biophysica* **2023**, *3*, 582–597. https://doi.org/10.3390/biophysica3040040

Academic Editor: Serge Perez

Received: 9 October 2023
Revised: 21 October 2023
Accepted: 27 October 2023
Published: 28 October 2023

1. Introduction

The Huntington protein, also known as huntingtin, is a large protein characterized by its solenoid architecture [1]. It is closely associated with the neurodegenerative disorder Huntington's disease (HD) [2–4]. Central to investigations into the molecular underpinnings of HD is the exploration of the structural and functional attributes of a polyglutamine tract located near the N-terminus of huntingtin [5–9]. Preceding the polyglutamine tract is a 17-residue fragment known as HttN, a dynamic and multifaceted region that has garnered significant attention. HttN plays a pivotal role in various cellular interactions [10] and post-translational modifications [11]. Unlike many other proteins, HttN lacks a well-defined globular domain due to its intrinsic disorder, allowing it to adopt multiple conformations [12–16], facilitating interactions with diverse cellular binding partners. Intriguingly, membrane association [17–19] or crystallization [20] of the N-terminal region can transform its disordered structure into an amphipathic α-helix.

HttN is subject to an array of post-translational modifications, including phosphorylation, acetylation, and palmitoylation [11]. Phosphorylation at specific serine and threonine residues within this region can modulate huntingtin's function, aggregation propensity, and cellular localization [21,22]. Conversely, acetylation regulates huntingtin's stability and interactions with other proteins and membranes [23,24]. These tightly regulated modifications influence huntingtin's behavior in both physiological and pathological contexts.

One of the striking features of huntingtin's N-terminus is its ability to associate with cellular membranes. This association has been observed with various membrane

compartments, including the endoplasmic reticulum (ER), Golgi apparatus, mitochondria, and synaptic membranes [10]. The presence of specific amino acid motifs within HttN, such as amphipathic helices, is believed to facilitate this interaction. These motifs allow huntingtin to bind to specific lipids within the membrane [25,26], thereby influencing its localization within these cellular structures.

HttN, when associated with membranes, features amphipathic segments characterized by the juxtaposition of hydrophobic and hydrophilic amino acids, a critical attribute for direct interactions with lipid membranes [17]. These interactions play a pivotal role in various cellular processes, including vesicle trafficking and membrane curvature modulation. Consequently, HttN's capacity to bind to and modify membrane properties bears significant implications for cellular physiology.

Dysregulated membrane interactions of HttN have been implicated in disrupted cellular processes in HD, spanning membrane trafficking, autophagy, and synaptic and mitochondrial functions [27]. Therefore, investigating membrane interactions with HttN is instrumental in advancing our understanding of HD pathogenesis. These interactions may hold the key to unraveling the mechanistic links between huntingtin dysfunction and neuronal dysfunction in the context of HD.

Extensive research has contributed valuable insights into HttN-mediated polyglutamine misfolding and toxicity [12,28–38], as well as its interactions with lipid bilayers [39]. The amphipathic nature of HttN has been revealed as pivotal for subcellular localization [10] and membrane anchoring [18,39] of huntingtin. Moreover, research has unveiled various facets of membrane interactions with HttN, encompassing binding affinity, predictive models for HttN positioning and conformation in lipid membranes, and their influence on lipid membrane order and structure [17–19,27,40–44]. However, a comprehensive understanding of the membrane structural alterations induced by HttN binding remains incomplete.

Atomic force microscopy (AFM) has emerged as a valuable technique for visualizing intricate membrane perturbations induced by external elements [45–47]. An example can be found in a recent review paper on applying AFM to study the reorganization of lipid bilayers treated with antimicrobial and lipopeptides [48]. AFM has also been broadly employed to investigate membrane interactions with polyglutamine-containing huntingtin fragments [38,39,49–53]. In addition to imaging, AFM-based force spectroscopy can be used to reveal the mechanical properties of lipid bilayers (see the review article for an example [54]). In our research, we harnessed the capabilities of liquid-based AFM to examine an assortment of macromolecules and their impact on the topographical and mechanical characteristics of lipid bilayers. Through our studies, we have unveiled a spectrum of membrane alterations, ranging from the formation of nanometer-sized pores [55], subtle interfacial indentations [56], the emergence of micrometer-sized perforations [57,58], and lipid clustering [59].

In this study, we specifically focus on the N-terminal region of huntingtin, HttN, with the primary objective of utilizing AFM to elucidate detailed changes in membrane topography resulting from the binding of HttN. Of particular interest is the role played by anionic lipids, cholesterol, and phosphatidylethanolamine (PE) lipids in mediating membrane responses to HttN exposure. Through AFM imaging, we present a dynamic spectrum of novel membrane structures arising from interactions with HttN. Additionally, we employ AFM-based force spectroscopy to investigate the impact of HttN on mechanical properties of lipid bilayers.

The lipid bilayer stands as a fundamental component within cellular membranes, providing a dynamic platform that orchestrates a myriad of biological processes. Notably, the composition of lipid bilayers exhibits significant variation across distinct cellular compartments, and this diversity wields profound influence over the behaviors exhibited by membrane-associated proteins. Hence, the imperative to unravel the intricate interplay between HttN and lipid bilayers of varying compositions becomes readily apparent. Moreover, it has been well-documented that lipids possessing different chemical compositions

have the capacity to modulate the aggregation propensity of huntingtin peptides [60,61]. Consequently, it is important to systematically investigate how HttN engages with lipid membranes characterized by diverse lipid compositions. Such an investigation holds the promise of yielding valuable insights into the molecular mechanisms underpinning the membrane-related functions of HttN.

2. Results

2.1. POPC Bilayers

We used AFM imaging to examine topographical changes in 1-palmitoyl-2-oleoyl-*sn*-glycero-3-phosphatidylcholine (POPC) bilayers induced by varying HttN concentrations. In Figure 1A, the control bilayer displayed a smooth surface. However, with the introduction of 2 μM HttN (Figure 1B), noticeable bilayer disruption became evident, characterized by the formation of isolated holes. Height profile measurements indicated a depth of ~2 nm for these holes. Note that the apparent depth of these holes can be influenced by parameters such as scan size and tip geometry. In previous high-resolution scans, we reported bilayer thicknesses of ~3 nm [56–58]. However, based on the apparent hole depth of 2 nm observed in this study, which surpasses half the bilayer's thickness, we can reasonably deduce that the holes induced by HttN traverse the entire bilayer.

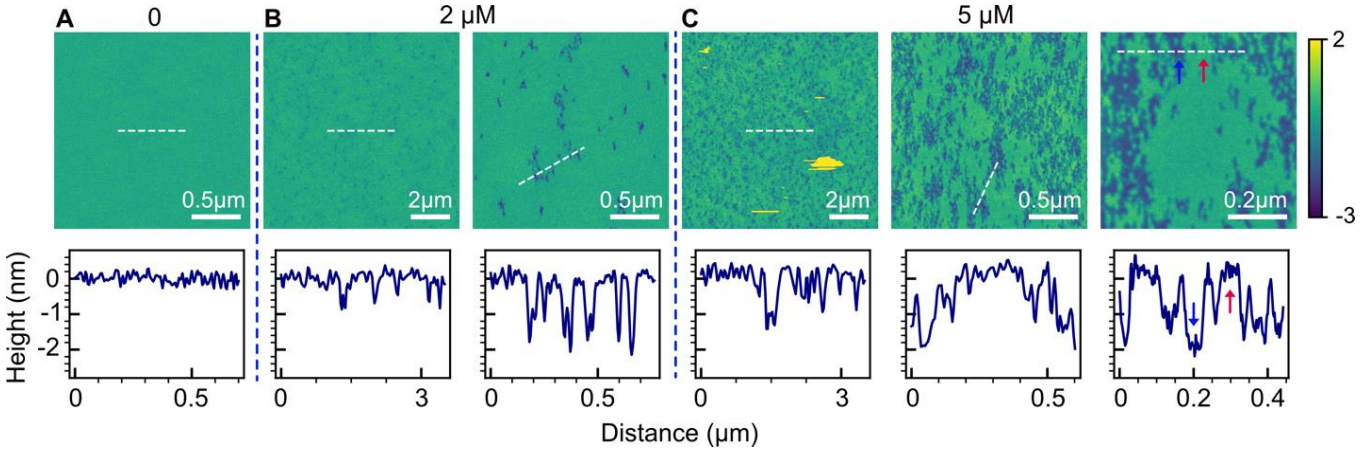

Figure 1. Perturbations of POPC bilayers exposed to varying concentrations of HttN. (**A**) 0 μM HttN, (**B**) 2 μM HttN, (**C**) 5 μM HttN. For 2 μM and 5 μM HttN, multiple images acquired at different scan sizes are presented. The scale bar indicates the size of each scan. Height scale is represented by the color bar on the right side, with units in nanometers (nm). The lower panels display height profiles along the white dashed lines depicted in the corresponding AFM images. The intact bilayer is marked by a red arrow, while the disrupted region is indicated by a blue arrow.

When the peptide concentration was increased to 5 μM, a considerable expansion in both the number and size of disrupted regions within the bilayer was observed. These disruptions no longer resembled isolated holes but rather irregularly shaped regions coexisting with the intact bilayer. It appeared that the peptide disrupted the POPC bilayer by extracting lipids, resulting in these irregularly shaped features, all with a consistent depth of ~2 nm, as confirmed by height profile measurements.

2.2. Effect of Anionic POPG Lipids

We further investigated the influence of anionic lipids on bilayer perturbations induced by HttN using a POPC/1-palmitoyl-2-oleoyl-*sn*-glycero-3-phosphoglycerol (POPG) (4:1, molar ratio) bilayer system. Figure 2 illustrates the effects of the peptide at a concentration of 2 μM. In contrast to the control bilayer, the addition of 2 μM HttN led to distinct bilayer alterations. These changes encompassed two key features: the formation of numerous holes in the main bilayer and the emergence of elevated bilayer patches. These elevated regions, referred to as 'double-bilayer patches,' were found to be elevated by 6 nm above

the main bilayer, as indicated by height profile measurements. Notably, isolated holes were also observed within these double-bilayer patches. The depth of holes was about 2 nm, similar to those observed in POPC bilayers. We also examined the impact of a 4 μM peptide concentration, but at this level, the majority of the POPC/POPG bilayer dissolved, resulting in messy scans.

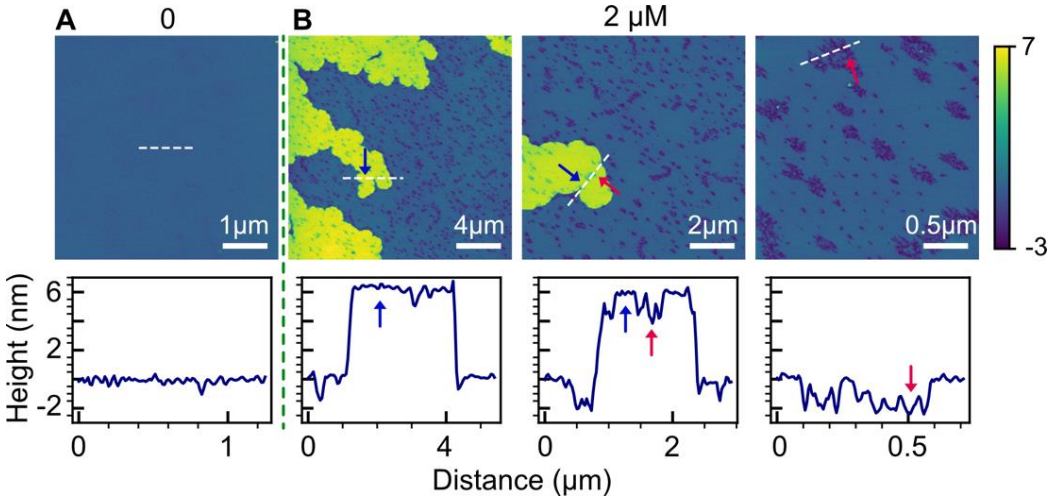

Figure 2. Influence of anionic POPG lipids on bilayer perturbations induced by HttN. The lipid bilayer comprises a mixture of POPC and POPG in a 4:1 molar ratio. Panels (**A**,**B**) depict bilayer structures before (**A**) and after (**B**) exposure to 2 μM HttN. Three images obtained at different scan sizes are provided for the 2 μM HttN condition. In the lower panels, height profiles along the white dashed lines, as indicated in the AFM images, are displayed. Disrupted bilayer regions are highlighted by red arrows, while elevated double-bilayer structures, measuring 6 nm in height above the main bilayer, are indicated by blue arrows.

We also utilized AFM-based force spectroscopy to further investigate the double-bilayer structures induced by HttN in POPC/POPG bilayers. Figure 3 presents the force spectroscopy results obtained before and after introducing 2 μM HttN. In Figure 3A, a composite of around 200 force curves is displayed, which were acquired while the AFM tip approached the bilayer and subsequently punctured it. The separation distance, denoted as 's', represents the distance between the AFM tip and the mica substrate.

During the approach phase (s > 6 nm), the force remains close to zero. Upon contact with the bilayer, the tip induces elastic deformation, leading to a gradual increase in force (as s decreases from 6 nm to 4 nm). Once the force reaches a threshold value, defined as the bilayer puncture force (Fp), the bilayer is punctured (s ≈ 4 nm). It is noteworthy that the puncture force serves as an indicator of the mechanical stability of lipid bilayers [54]. Within the regime of bilayer elastic deformation, we observe a continuous increase in force, following a power-law trend. For the control POPC/POPG bilayer, the average bilayer puncture force is measured at 1.6 ± 0.1 nN.

Following the addition of 2 μM HttN, we acquired about 200 force curves from regions within the main bilayer, as shown in Figure 3B. The average bilayer puncture force exhibited an increase to 1.8 ± 0.1 nN, suggesting an enhanced mechanical stability of the lipid bilayer. Additionally, the location of bilayer puncture shifted from s = 3.5 nm for the control bilayer to s = 3.2 nm with 2 μM HttN. We also obtained about 200 force curves from regions within the double-bilayer patches, as depicted in Figure 3C. Two bilayer puncture events were observed. The first puncture event, centered at s = 3.3 nm, had an average puncture force of 1.9 ± 0.1 nN, and the same average puncture force (1.9 ± 0.2 nN) was observed at the second puncture event, located at s = 8.8 nm. The distance between the two puncture events, 5.5 nm, aligned well with the height of the double-bilayer patches. Based on the identical puncture force between the two puncture events and the similarity in the elastic

deformation behaviors preceding them, it was apparent that the double-bilayer patches corresponded to a second bilayer residing atop the main bilayer.

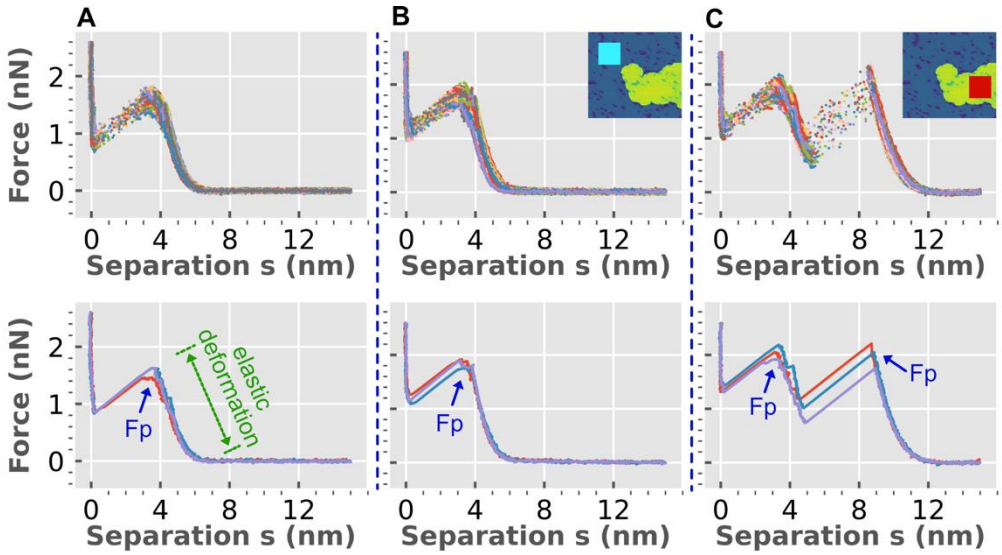

Figure 3. Force spectroscopy reveals alterations in mechanical properties of lipid bilayers induced by HttN. (**A**) Force spectroscopy data of a POPC/POPG (4:1) bilayer before exposure to HttN and (**B**,**C**) after exposure to 2 μM HttN. Panel (**B**) presents force measurements in the main bilayer region, while panel (**C**) displays force measurements in the double-bilayer region. The single and double-bilayer regions are illustrated in the inset images in (**B**,**C**) by cyan and red boxes, respectively. Each panel in the top row depicts a superposition of ~200 force curves. In the bottom panels, three representative force curves are shown. The bilayer puncture force (Fp) is indicated at a separation distance (s) of ~4 nm for the single bilayer and ~8 nm for the double bilayer. Within the elastic deformation regime (as s decreases from 6 nm to 4 nm in single bilayers), the force steadily increases until reaching the puncture force.

2.3. Effect of Anionic Cardiolipin Lipids

To further investigate the influence of anionic lipids, we introduced a doubly charged cardiolipin lipid, 1′,3′-bis[1,2-dioleoyl-*sn*-glycero-3-phospho]-*sn*-glycerol (TOCL), into the bilayer composition along with POPC. Cardiolipin lipids are unique and are typically found in the mitochondria of eukaryotic cells. Figure 4 displays the bilayer topology of POPC/TOCL (9:1, molar ratio) before and after the addition of 2 μM HttN. Similar to the observations in POPC/POPG bilayers, HttN induced the formation of double-bilayer patches situated atop the main bilayer, elevated by 6 nm. Peptide-induced holes were also evident in both the main bilayer and the elevated patches, with a depth of about 2.5 nm.

2.4. Effect of Cholesterol

To assess the impact of cholesterol (Chol), we employed a POPC/Chol bilayer system with cholesterol mole fractions ranging from 0% to 40%. Figure 5 presents the topographical structures of POPC/Chol bilayers treated with 2 μM HttN. Notably, as the cholesterol fraction increased, the extent of bilayer perturbation became more pronounced, as indicated by hole size, albeit some heterogeneity was observed at all cholesterol fractions. Additionally, our data analysis revealed that the hole area coverage was smaller at lower cholesterol content (0.02 for 0% and 10% cholesterol) and larger at higher cholesterol content (0.04 for 20%, 30%, and 40% cholesterol). These findings emphasize that higher cholesterol content in POPC bilayers results in more significant alterations of bilayer structures induced by HttN. Height profile measurements indicated hole depths of ~3 nm. Note that for POPC with 0% cholesterol, the holes were too small for precise measurement; more accurate hole depths can be found in Figure 1.

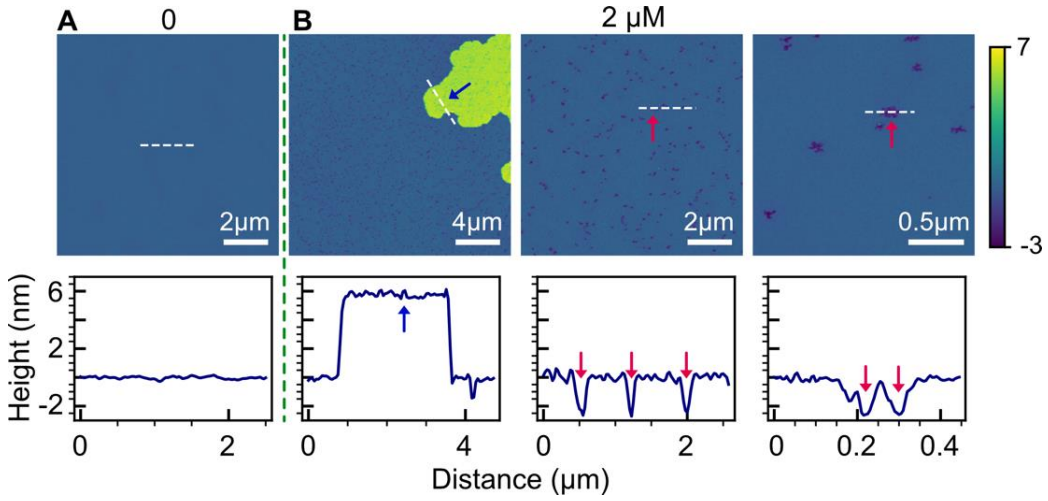

Figure 4. Impact of anionic cardiolipin lipids on bilayer responses to HttN binding. The lipid bilayer consists of a mixture of POPC and TOCL in a 9:1 molar ratio. Panels (**A**,**B**) represent bilayer structures before (**A**) and after (**B**) exposure to 2 μM HttN. Three images obtained at different scan sizes are provided for the 2 μM HttN condition. In the lower panels, height profiles along the white dashed lines, as indicated in the AFM images, are displayed. Disrupted bilayer regions are highlighted by red arrows, while elevated double-bilayer structure, measuring 6 nm in height above the main bilayer, is indicated by a blue arrow.

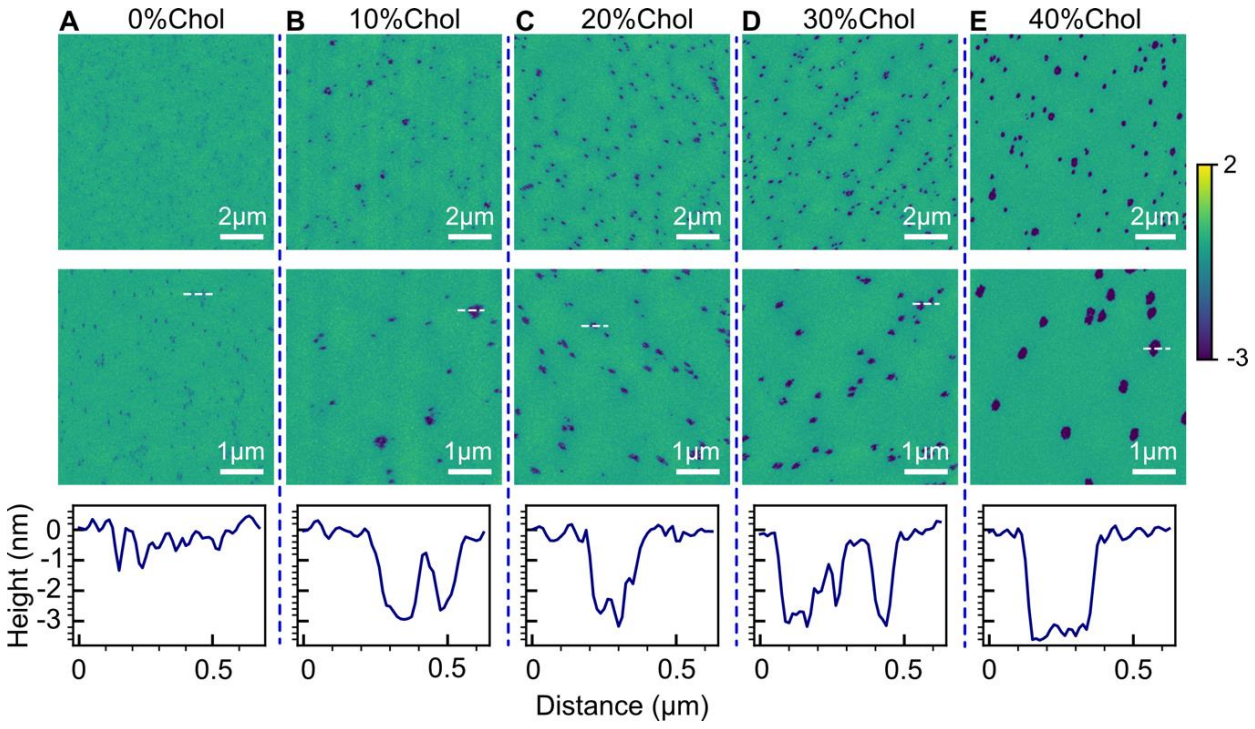

Figure 5. Influence of cholesterol content on bilayer alterations induced by 2 μM HttN. The bilayer compositions investigated include (**A**) POPC, (**B**) POPC with 10 mol% Chol, (**C**) POPC with 20 mol% Chol, (**D**) POPC with 30 mol% Chol, and (**E**) POPC with 40 mol% Chol. Two AFM images, acquired at different scan sizes, are presented for each lipid composition. The bottom panels illustrate height profiles along the white dashed lines shown in the AFM images from the second row.

For POPC bilayers containing 30% and 40% cholesterol, in addition to hole formation, HttN also induced the appearance of double-bilayer patches, as shown in Figure 6. Height profile measurements revealed that these double-bilayer patches had a height of 6.7 nm

above the main bilayer. The presence of double-bilayer patches in anionic POPC/POPG and POPC/TOCL bilayers, as well as in POPC bilayers with high cholesterol contents, suggests that both anionic lipids and cholesterol contribute to the formation of double-bilayer patches induced by HttN.

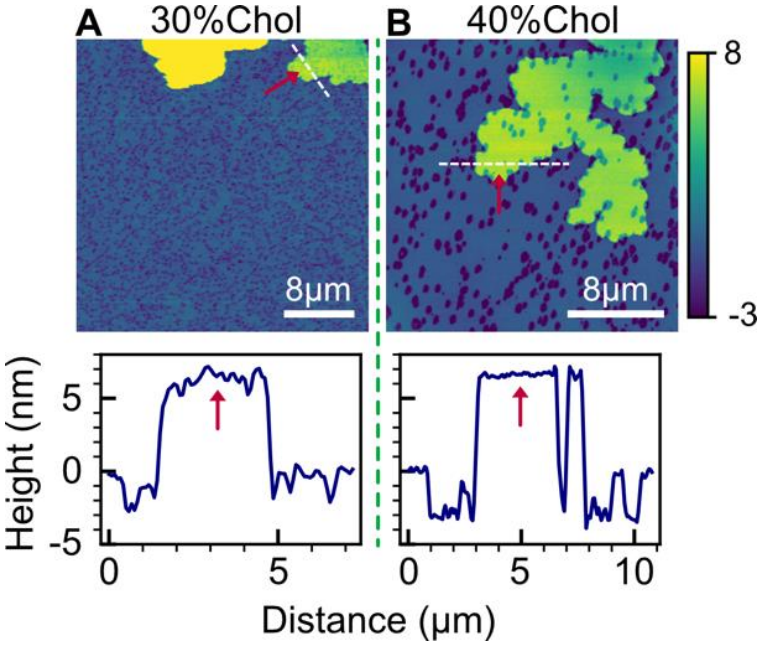

Figure 6. Formation of double-bilayer patches induced by 2 μM HttN in bilayers with elevated cholesterol concentrations. The bilayer compositions used are as follows: (**A**) POPC with 30 mol% cholesterol and (**B**) POPC with 40 mol% cholesterol. The lower panels display height profiles along the white dashed lines in the AFM images, with the double-bilayer patches, elevated by 6.7 nm above the main bilayer, indicated by red arrows. The yellow patch in (**A**) has a height of about 13 nm.

2.5. Effect of POPE

PE lipids possess a conical shape and are believed to enhance membrane stability by forming hydrogen bonds with neighboring lipids. To assess the impact of HttN on POPC bilayers with varying fractions of 1-palmitoyl-2-oleoyl-*sn*-glycero-3-phosphatidylethanolamine (POPE), we employed a peptide concentration of 5 μM. The results are presented in Figure 7.

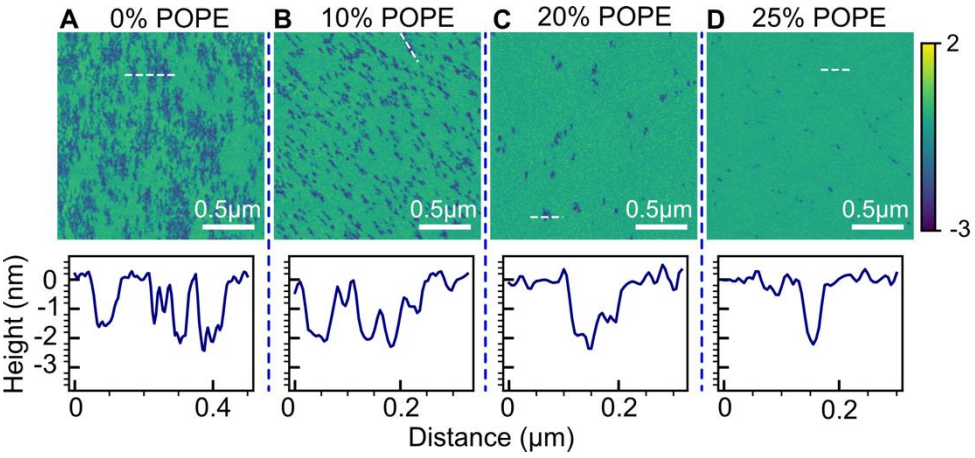

Figure 7. Influence of POPE content on bilayer modulations induced by 5 μM HttN. Lipid bilayer compositions: (**A**) POPC, (**B**) POPC with 10 mol% POPE, (**C**) POPC with 20 mol% POPE, (**D**) POPC with 25 mol% POPE. The lower panels display height profiles along the white dashed lines marked in the AFM images.

As the POPE mole fraction increased from 0% to 10%, a notable suppression of bilayer hole formation was observed. This was substantiated by data analysis, which revealed that the hole area coverage decreased from 0.35 at 0% POPE to 0.16 at 10% POPE. A significant suppression of hole formation was also observed when the POPE content increased from 10% to 20%, with the hole area coverage decreasing from 0.16 to 0.03. At 25% POPE, only holes with miniscule sizes were observed. Height profile measurements indicated that hole depths were about 2 nm across all POPE contents.

3. Discussion

In this investigation, we explored the intricate interplay between HttN and lipid bilayers of varying compositions. Our study utilized lipid-based AFM to scrutinize the topographical alterations induced by HttN in different lipid environments, revealing consistent trends across multiple lipid compositions. Notably, we observed that the peptide induced bilayer perturbations by forming holes. Moreover, we uncovered the pivotal role of lipid specificity in modulating these perturbations, along with the intriguing emergence of elevated double-bilayer patches in the presence of anionic lipids and high cholesterol concentrations.

3.1. Bilayer Hole Formation

One of the prominent findings in our study is the formation of holes within lipid bilayers. This observation underscores an essential aspect of HttN's interaction with lipid membranes, emphasizing its ability to disrupt lipid bilayers by extracting lipids from regions of perturbation. In line with our observation, previous studies have reported HttN-induced dye leakage from lipid vesicles [40]. As HttN interacts with lipid bilayers, it destabilizes local lipid packing or positioning, leading to the formation of voids within the membrane. This behavior shares similarities with the action of detergents, known for their lipid-extraction properties. HttN's ability to create holes within the bilayer suggests that it may act as a molecular detergent, disrupting membrane integrity through lipid extraction. The enhanced interactions with acidic lipids [25] can explain the increased hole occurrence observed in the presence of POPG or cardiolipin. In contrast to the POPC bilayer, the holes observed in POPC/cholesterol bilayers displayed a higher degree of discreteness and featured well-defined perimeters (Figure 1 compared with Figure 5). This difference is likely attributed to the effect of cholesterol on the physical properties of lipid bilayers, such as bilayer thickness and chain order.

3.2. Implications of Force Spectroscopy

In POPC/POPG bilayers, our AFM-based force spectroscopy revealed that HttN increased the bilayer puncture force and induced a shift in the puncture position. The increase in bilayer puncture force implies that peptide binding enhances bilayer resistance to mechanical perturbations. This could be caused by interactions between the peptide and surrounding lipid molecules. Changes in the puncture position can be associated with bilayer thickness. For instance, a decrease in the puncture position reflects a bilayer thinning effect impacted by ethanol [62]. Given that HttN decreased the puncture position from s = 3.5 nm to 3.2 nm, it could imply that the peptide slightly reduced the bilayer thickness.

3.3. Effect of Cholesterol

Modulations in cholesterol homeostasis have been implicated in HD [63–65]. Additionally, biophysical investigations have elucidated the role of cholesterol in modifying huntingtin's membrane interactions [66]. Our AFM study has unveiled useful insights into the role of cholesterol in membrane dynamics. A striking positive correlation was found between cholesterol concentration and the extent of hole formation induced by HttN. Specifically, the presence of cholesterol fosters the formation of bilayer holes, accompanied by an augmentation in the size and area coverage of these openings as cholesterol con-

centration increases. This dose-dependent relationship underscores the intricate interplay between cholesterol and HttN within the membrane.

Cholesterol is known for its capacity to influence membrane properties by modulating lipid packing and ordering [67–69]. In the context of our investigation, it is conceivable that cholesterol enhances the disruption of lipid–lipid interactions initiated by HttN. The rigid and planar structure of cholesterol may introduce localized defects within the lipid bilayer, facilitating the insertion of HttN and subsequent lipid extraction. This perturbation in lipid organization, instigated by cholesterol, could potentially amplify the destabilizing effects of HttN, leading to a higher propensity for hole formation.

Cholesterol holds a prominent role in neuronal membranes, where it actively contributes to membrane fluidity and the organization of lipid rafts [70]. Consequently, the observed influence of cholesterol on HttN-induced hole formation bears implications for neuronal membrane integrity and functionality. Cholesterol-induced holes may disrupt the compartmentalization of membrane proteins and lipids within lipid rafts, potentially impacting crucial cellular processes. The altered membrane properties could compromise the function of membrane-associated proteins, including huntingtin and other interacting partners.

3.4. Effect of POPE

Our investigation into the influence of PE lipids (specifically, POPE) on hole formation has revealed intriguing insights into the role of these lipids in modulating membrane dynamics. A notable reduction in hole formation was observed with increasing POPE content within the bilayer. Higher POPE concentrations correlated with fewer holes and a diminished hole area coverage, shedding light on the regulatory potential of PE lipids in mitigating the disruptive effects of HttN. A similar result demonstrating the inhibitory effect of PE lipids on HttN-membrane interactions has been reported through molecular simulations [44].

PE lipids, which constitute a significant portion of total phospholipids in mammalian cells, possess a distinctive conical shape, distinguishing them from other lipid species present in cellular membranes. This unique geometry has been associated with stabilizing membrane structures by promoting negative spontaneous curvature [71] and enhanced lipid packing. The inverse relationship between PE concentration and hole formation suggests that PE's conical shape and capacity to enhance membrane stability may inhibit HttN's propensity to induce structural perturbations within the lipid bilayer.

The biological implications of PE-mediated regulation of hole formation are multifaceted. Our findings suggest that PE lipids may serve as natural modulators, tempering the destabilizing effects of the N-terminal region of huntingtin within neuronal membranes. This regulatory role of PE lipids could play a crucial part in maintaining the integrity of membrane-bound proteins and lipid domains. In the context of HD, where membrane dysfunction is implicated, PE's capacity to reduce hole formation may offer a protective mechanism against the structural disruptions associated with the disease.

3.5. Double-Bilayer Patches

One of the prominent findings in our study is the appearance of double-bilayer patches in bilayers containing anionic lipids (POPG and TOCL) or high contents of cholesterol. These patches, characterized by a second bilayer elevated above the main bilayer, point to the propensity of these lipid compositions to undergo bilayer fusion. Interestingly, we also observed double-bilayer patches in our previous investigation involving a peptidomimetic [72]. Further supporting our interpretation of the elevated patch as a second bilayer are the similar two-puncture events observed in force spectroscopy for a double-bilayer system formed by tethering two bilayers together [73].

Height measurements revealed that the elevated patches had a height of near 6 nm, exceeding the thickness of the main bilayer (as seen in Figure 5E, which is 3.7 nm thick). However, the elevated patch cannot be attributed to two bilayers because only one additional puncture event was observed in our force spectroscopy measurements (Figure 3). One possible explanation for the 6 nm thickness of the elevated patch was the presence of a water layer separating it from the main bilayer. Such a situation is not uncommon, as water spacing typically exists between neighboring bilayers in multilamellar vesicles. Indeed, previous studies employing X-ray diffraction have reported a repeating spacing of about 6 nm in multilamellar vesicles [74,75]. These findings may elucidate the observed 6 nm thickness of the elevated patches in our study.

The formation of double-bilayer patches suggests that anionic lipids and cholesterol can promote bilayer fusion, potentially by facilitating lipid mixing between adjacent bilayers. Anionic lipids, such as POPG and TOCL, carry a net negative charge due to their head groups, which can interact favorably with cationic regions of HttN. These electrostatic interactions may bring the bilayers closer together, enhancing the tendency of bilayer fusion. Additionally, cholesterol's ability to modulate membrane fluidity and ordering may play a role in promoting bilayer fusion. By inducing localized negative curvature in the bilayer [76] and affecting lipid packing, cholesterol may facilitate the merger of adjacent bilayers and the formation of double-bilayer patches.

It is noteworthy that a broad spectrum of amphipathic peptides has been shown to exhibit fusogenic properties [77–81]. Due to the fusion tendency facilitated by HttN, anionic lipids, and cholesterol, the extracted lipids can form complexes with the peptide, which can fuse onto existing bilayer surfaces to form the observed double-bilayer patches.

3.6. Implications of Bilayer Fusion

The propensity for membrane fusion, exemplified by the formation of double-bilayer patches mediated by HttN, anionic lipids, and cholesterol, holds significant biological relevance, particularly within the contexts of synaptic vesicle trafficking and mitochondrial dynamics. In synaptic vesicle trafficking, the fusion of synaptic vesicles with the presynaptic membrane involves membrane reorganization. Our findings demonstrate that interactions between the N-terminal region of huntingtin and anionic lipids and cholesterol can enhance bilayer fusion. The presence of double-bilayer patches within neuronal membranes may impact the distribution and localization of synaptic vesicle fusion sites, potentially influencing neurotransmitter release efficiency. Disrupted synaptic vesicle trafficking is associated with HD [82,83], underscoring the relevance of our findings in elucidating the mechanisms underlying synaptic dysfunction in this disease.

Mitochondrial dysfunction is considered a contributing factor in HD pathogenesis [84–86]. Membrane fusion, facilitated by interactions between anionic cardiolipin lipids and the N-terminal region of huntingtin, may have profound implications for mitochondrial dynamics. Mitochondrial fusion events involve the merging of mitochondrial outer membranes, a process resembling bilayer fusion. The heightened propensity for bilayer fusion in the presence of cardiolipin and HttN may influence the dynamics of mitochondrial fusion events, potentially resulting in compromised energy production and deficits in neuronal viability (prominent features of HD pathology) [87–91].

3.7. Implications of Lipid Specificity

The lipid bilayer is an essential component of cellular membranes, playing a pivotal role in maintaining cellular integrity and function. Our study highlights the influence of lipid composition on the interactions between the N-terminal region of huntingtin and lipid membranes. The specificity of lipid interactions observed in this study, such as the formation of holes and double-bilayer patches, emphasizes the importance of considering the lipid environment when investigating membrane-associated proteins.

HD is characterized by the accumulation of mutant huntingtin in various cellular compartments, including the endoplasmic reticulum, Golgi apparatus, and mitochondria. The selective vulnerability of specific neuronal populations in this disease may be linked to the distinct lipid composition of their membranes, influencing the interaction of mutant huntingtin with these membranes. Our results raise intriguing possibilities regarding the role of lipid-specific interactions in the intracellular trafficking, aggregation, and toxicity of mutant huntingtin.

4. Materials and Methods

Lipids including 1-palmitoyl-2-oleoyl-*sn*-glycero-3-phosphatidylcholine (POPC), 1-palmitoyl-2-oleoyl-*sn*-glycero-3-phosphoglycerol (POPG), 1-palmitoyl-2-oleoyl-*sn*-glycero-3-phosphatidylethanolamine (POPE), cholesterol (Chol), and cardiolipin 1′,3′-bis[1,2-dioleoyl-*sn*-glycero-3-phospho]-*sn*-glycerol (TOCL) were purchased from Avanti Polar Lipids (Alabaster, AL, USA). HttN was purchased in powder form from GenScript Biotech (Piscataway, NJ, USA) with a reported purity of 94%. The peptide sequence is as follows: MATLEKLMKAFESLKSFQQQ-NH_2, where three glutamine residues are included to facilitate a smooth transition from the N-terminal region to the polyglutamine tract. The peptide is denoted as HttN. All percentages and ratios presented in this paper are molar-based.

Lipid stocks were prepared by dissolving lipid powder in either chloroform or a chloroform/methanol mixture. To prepare lipid samples with different compositions, appropriate volumes of lipid stocks were mixed in glass test tubes. The organic solvents were evaporated using a 12-position N-EVAP evaporator from Organomation Associates, Inc. (Berlin, MA, USA). Further removal of organic solvents was achieved by subjecting lipid films to vacuum pumping. Lipid dry films were hydrated using Milli-Q water containing 5 mM calcium chloride. Small unilamellar vesicles (SUVs) were then generated utilizing a Branson Ultrasonic Sonifier SFX 250 equipped with a flat tip. The obtained SUV solution was briefly centrifuged before bilayer preparation.

AFM experiments were conducted using a liquid-compatible Multimode 8 AFM controlled by a Nanoscope V controller (Bruker, Santa Barbara, CA, USA), with the liquid cell (MTFML-V2 from Bruker) employed for peptide–bilayer interactions. The experimental procedure has been reported previously [92–94]. In brief, 200 µL of SUV solution was injected into the liquid cell, leading to the formation of a mica-supported planar bilayer. Excess SUVs were flushed out after bilayer formation. Silicon nitride probes (Bruker DNP-S10 tip A, spring constant ~0.3 N/m) were used for both imaging and force spectroscopy. Imaging was carried out in PeakForce quantitative nanomechanical (QNM) mode, with a peak-force of ~400 pN. Subsequently, peptide solutions containing various concentrations of HttN were slowly introduced into the liquid cell using a syringe pump. Imaging was conducted after about 10 min of incubation of the peptide with the lipid bilayer, with the peptide concentration maintained consistently in the liquid cell. Multiple regions of the bilayer surface were scanned for both the control and peptide-treated bilayers to obtain an averaged perspective. Each lipid composition experiment was conducted on at least two separate occasions to ensure the consistency of our results.

For AFM-based force spectroscopy, the same bilayer preparation and peptide introduction methods were followed. Initial imaging was conducted to locate regions for force measurements. Force ramping was performed at multiple points using the point-and-shoot function provided by the Nanoscope software. Custom Python scripts were used to analyze and display the acquired AFM images and force spectroscopy data.

5. Conclusions

In this study, we conducted a comprehensive investigation into the topographical alterations induced by the N-terminal region of huntingtin within lipid bilayers of varying compositions. Our results reveal intriguing insights into the interplay between HttN and lipid bilayers, shedding light on the mechanisms underlying bilayer perturbations. Notably, we observed bilayer disruptions in all lipid compositions tested, characterized by the emergence of transmembrane holes within the bilayers. The extent of these disruptions was mediated by the lipid environment, with the presence of anionic lipids, cholesterol, and PE lipids playing pivotal roles in modulating bilayer responses to HttN. Additionally, the formation of double-bilayer patches was identified as a distinct phenomenon in the presence of anionic lipids and high cholesterol contents, suggesting a fusogenic property of these components. These findings emphasize the intricate relationship between lipid composition and the interaction of HttN with lipid bilayers. Such insights are crucial for our understanding of the molecular mechanisms underlying HD pathogenesis. Our study underscores the importance of considering lipid heterogeneity in biophysical investigations of membrane-associated proteins, as lipid composition plays a critical role in shaping the bilayer responses to protein-induced perturbations.

Author Contributions: J.P. conceptualized the project; Y.I.G. and J.P. conducted the experiments and analyzed the data; J.P. wrote the manuscript. All authors have read and agreed to the published version of the manuscript.

Funding: This research was supported by the National Institutes of Health Award Number 1R03NS1-35210-01 to J.P.

Data Availability Statement: Data available on request.

Conflicts of Interest: The authors declare no conflict of interest.

References

1. Vijayvargia, R.; Epand, R.; Leitner, A.; Jung, T.Y.; Shin, B.; Jung, R.; Lloret, A.; Atwal, R.S.; Lee, H.; Lee, J.M.; et al. Huntingtin's spherical solenoid structure enables polyglutamine tract-dependent modulation of its structure and function. *eLife* **2016**, *5*, e11184. [CrossRef]
2. Saudou, F.; Humbert, S. The Biology of Huntingtin. *Neuron* **2016**, *89*, 910–926.
3. Zuccato, C.; Valenza, M.; Cattaneo, E. Molecular Mechanisms and Potential Therapeutical Targets in Huntington's Disease. *Physiol. Rev.* **2010**, *90*, 905–981. [CrossRef]
4. Jurcau, A. Molecular Pathophysiological Mechanisms in Huntington's Disease. *Biomedicines* **2022**, *10*, 1432. [CrossRef]
5. Zoghbi, H.Y.; Orr, H.T. Glutamine repeats and neurodegeneration. *Annu. Rev. Neurosci.* **2000**, *23*, 217–247. [CrossRef]
6. Bauer, P.O.; Nukina, N. The pathogenic mechanisms of polyglutamine diseases and current therapeutic strategies. *J. Neurochem.* **2009**, *110*, 1737–1765. [CrossRef]
7. Gusella, J.F.; MacDonald, M.E. Molecular genetics: Unmasking polyglutamine triggers in neurodegenerative disease. *Nat. Rev. Neurosci.* **2000**, *1*, 109–115.
8. Takahashi, T.; Katada, S.; Onodera, O. Polyglutamine Diseases: Where does Toxicity Come from? What is Toxicity? Where are We Going? *J. Mol. Cell Biol.* **2010**, *2*, 180–191. [CrossRef]
9. Wetzel, R. Physical Chemistry of Polyglutamine: Intriguing Tales of a Monotonous Sequence. *J. Mol. Biol.* **2012**, *421*, 466–490.
10. Rockabrand, E.; Slepko, N.; Pantalone, A.; Nukala, V.N.; Kazantsev, A.; Marsh, J.L.; Sullivan, P.G.; Steffan, J.S.; Sensi, S.L.; Thompson, L.M. The first 17 amino acids of Huntingtin modulate its sub-cellular localization, aggregation and effects on calcium homeostasis. *Hum. Mol. Genet.* **2007**, *16*, 61–77. [CrossRef]
11. Ehrnhoefer, D.E.; Sutton, L.; Hayden, M.R. Small Changes, Big Impact: Posttranslational Modifications and Function of Huntingtin in Huntington Disease. *Neuroscientist* **2011**, *17*, 475–492. [CrossRef] [PubMed]
12. Thakur, A.K.; Jayaraman, M.; Mishra, R.; Thakur, M.; Chellgren, V.M.; Byeon, I.J.L.; Anjum, D.H.; Kodali, R.; Creamer, T.P.; Conway, J.F.; et al. Polyglutamine disruption of the huntingtin exon 1 N terminus triggers a complex aggregation mechanism. *Nat. Struct. Mol. Biol.* **2009**, *16*, 380–389. [CrossRef] [PubMed]
13. Kim, M.W.; Chelliah, Y.; Kim, S.W.; Otwinowski, Z.; Bezprozvanny, I. Secondary Structure of Huntingtin Amino-Terminal Region. *Structure* **2009**, *17*, 1205–1212. [CrossRef] [PubMed]

14. Rossetti, G.; Cossio, P.; Laio, A.; Carloni, P. Conformations of the Huntingtin N-term in aqueous solution from atomistic simulations. *FEBS Lett.* **2011**, *585*, 3086–3089. [CrossRef] [PubMed]
15. Dlugosz, M.; Trylska, J. Secondary Structures of Native and Pathogenic Huntingtin N-Terminal Fragments. *J. Phys. Chem. B* **2011**, *115*, 11597–11608. [CrossRef] [PubMed]
16. Binette, V.; Cote, S.; Mousseau, N. Free-Energy Landscape of the Amino-Terminal Fragment of Huntingtin in Aqueous Solution. *Biophys. J.* **2016**, *110*, 1075–1088. [CrossRef]
17. Michalek, M.; Salnikov, E.S.; Bechinger, B. Structure and Topology of the Huntingtin 1–17 Membrane Anchor by a Combined Solution and Solid-State NMR Approach. *Biophys. J.* **2013**, *105*, 699–710. [CrossRef]
18. Cote, S.; Binette, V.; Salnikov, E.S.; Bechinger, B.; Mousseau, N. Probing the Huntingtin 1–17 Membrane Anchor on a Phospholipid Bilayer by Using All-Atom Simulations. *Biophys. J.* **2015**, *108*, 1187–1198. [CrossRef]
19. Tao, M.X.; Pandey, N.K.; Barnes, R.; Han, S.; Langen, R. Structure of Membrane-Bound Huntingtin Exon 1 Reveals Membrane Interaction and Aggregation Mechanisms. *Structure* **2019**, *27*, 1570–1580. [CrossRef]
20. Kim, M. Beta conformation of polyglutamine track revealed by a crystal structure of Huntingtin N-terminal region with insertion of three histidine residues. *Prion* **2013**, *7*, 221–228. [CrossRef]
21. Cariulo, C.; Azzollini, L.; Verani, M.; Martufi, P.; Boggio, R.; Chiki, A.; Deguire, S.M.; Cherubini, M.; Gines, S.; Marsh, J.L.; et al. Phosphorylation of huntingtin at residue T3 is decreased in Huntington's disease and modulates mutant huntingtin protein conformation. *Proc. Natl. Acad. Sci. USA* **2017**, *114*, E10809–E10818. [CrossRef] [PubMed]
22. DeGuire, S.M.; Ruggeri, F.S.; Fares, M.B.; Chiki, A.; Cendrowska, U.; Dietler, G.; Lashuel, H.A. N-terminal Huntingtin (Htt) phosphorylation is a molecular switch regulating Htt aggregation, helical conformation, internalization, and nuclear targeting. *J. Biol. Chem.* **2018**, *293*, 18540–18558. [CrossRef] [PubMed]
23. Monsellier, E.; Redeker, V.; Ruiz-Arlandis, G.; Bousset, L.; Melki, R. Molecular Interaction between the Chaperone Hsc70 and the N-terminal Flank of Huntingtin Exon 1 Modulates Aggregation. *J. Biol. Chem.* **2015**, *290*, 2560–2576. [CrossRef] [PubMed]
24. Chaibva, M.; Jawahery, S.; Pilkington, A.W.; Arndt, J.R.; Sarver, O.; Valentine, S.; Matysiak, S.; Legleiter, J. Acetylation within the First 17 Residues of Huntingtin Exon 1 Alters Aggregation and Lipid Binding. *Biophys. J.* **2016**, *111*, 349–362. [CrossRef]
25. Kegel, K.B.; Sapp, E.; Yoder, J.; Cuiffo, B.; Sobin, L.; Kim, Y.J.; Qin, Z.H.; Hayden, M.R.; Aronin, N.; Scott, D.L.; et al. Huntingtin associates with acidic phospholipids at the plasma membrane. *J. Biol. Chem.* **2005**, *280*, 36464–36473. [CrossRef]
26. Kegel, K.B.; Sapp, E.; Alexander, J.; Valencia, A.; Reeves, P.; Li, X.Y.; Masso, N.; Sobin, L.; Aronin, N.; DiFiglia, M. Polyglutamine expansion in huntingtin alters its interaction with phospholipids. *J. Neurochem.* **2009**, *110*, 1585–1597. [CrossRef]
27. Nagarajan, A.; Jawahery, S.; Matysiak, S. The Effects of Flanking Sequences in the Interaction of Polyglutamine Peptides with a Membrane Bilayer. *J. Phys. Chem. B* **2014**, *118*, 6368–6379. [CrossRef]
28. Duennwald, M.L.; Jagadish, S.; Muchowski, P.J.; Lindquist, S. Flanking sequences profoundly alter polyglutamine toxicity in yeast. *Proc. Natl. Acad. Sci. USA* **2006**, *103*, 11045–11050. [CrossRef]
29. Atwal, R.S.; Xia, J.; Pinchev, D.; Taylor, J.; Epand, R.M.; Truant, R. Huntingtin has a membrane association signal that can modulate huntingtin aggregation, nuclear entry and toxicity. *Hum. Mol. Genet.* **2007**, *16*, 2600–2615. [CrossRef]
30. Jayaraman, M.; Kodali, R.; Sahoo, B.; Thakur, A.K.; Mayasundari, A.; Mishra, R.; Peterson, C.B.; Wetzel, R. Slow Amyloid Nucleation via alpha-Helix-Rich Oligomeric Intermediates in Short Polyglutamine-Containing Huntingtin Fragments. *J. Mol. Biol.* **2012**, *415*, 881–899. [CrossRef]
31. Sivanandam, V.N.; Jayaraman, M.; Hoop, C.L.; Kodali, R.; Wetzel, R.; van der Wel, P.C.A. The Aggregation-Enhancing Huntingtin N-Terminus Is Helical in Amyloid Fibrils. *J. Am. Chem. Soc.* **2011**, *133*, 4558–4566. [CrossRef] [PubMed]
32. Hoop, C.L.; Lin, H.K.; Kar, K.; Hou, Z.P.; Poirier, M.A.; Wetzel, R.; van der Wel, P.C.A. Polyglutamine Amyloid Core Boundaries and Flanking Domain Dynamics in Huntingtin Fragment Fibrils Determined by Solid-State Nuclear Magnetic Resonance. *Biochemistry* **2014**, *53*, 6653–6666. [CrossRef] [PubMed]
33. Williamson, T.E.; Vitalis, A.; Crick, S.L.; Pappu, R.V. Modulation of Polyglutamine Conformations and Dimer Formation by the N-Terminus of Huntingtin. *J. Mol. Biol.* **2010**, *396*, 1295–1309. [CrossRef] [PubMed]
34. Veldman, M.B.; Rios-Galdamez, Y.; Lu, X.H.; Gu, X.F.; Qin, W.; Li, S.; Yang, X.W.; Lin, S. The N17 domain mitigates nuclear toxicity in a novel zebrafish Huntington's disease model. *Mol. Neurodegener.* **2015**, *10*, 67. [CrossRef]
35. Gu, X.F.; Cantle, J.P.; Greiner, E.R.; Lee, C.Y.D.; Barth, A.M.; Gao, F.Y.; Park, C.S.; Zhang, Z.Q.; Sandoval-Miller, S.; Zhang, R.L.; et al. N17 Modifies Mutant Huntingtin Nuclear Pathogenesis and Severity of Disease in HD BAC Transgenic Mice. *Neuron* **2015**, *85*, 726–741. [CrossRef]
36. Pandey, N.K.; Isas, J.M.; Rawat, A.; Lee, R.V.; Langen, J.; Pandey, P.; Langen, R. The 17-residue-long N terminus in huntingtin controls stepwise aggregation in solution and on membranes via different mechanisms. *J. Biol. Chem.* **2018**, *293*, 2597–2605. [CrossRef]
37. Lakhani, V.V.; Ding, F.; Dokholyan, N.V. Polyglutamine Induced Misfolding of Huntingtin Exon1 is Modulated by the Flanking Sequences. *PLoS Comput. Biol.* **2010**, *6*, e1000772. [CrossRef]
38. Huynen, C.; Willet, N.; Buell, A.K.; Duwez, A.S.; Jerome, C.; Dumoulin, M. Influence of the protein context on the polyglutamine length-dependent elongation of amyloid fibrils. *BBA Proteins Proteom.* **2015**, *1854*, 239–248. [CrossRef]

39. Burke, K.A.; Kauffman, K.J.; Umbaugh, C.S.; Frey, S.L.; Legleiter, J. The Interaction of Polyglutamine Peptides with Lipid Membranes Is Regulated by Flanking Sequences Associated with Huntingtin. *J. Biol. Chem.* **2013**, *288*, 14993–15005. [CrossRef]
40. Michalek, M.; Salnikov, E.S.; Werten, S.; Bechinger, B. Membrane Interactions of the Amphipathic Amino Terminus of Huntingtin. *Biochemistry* **2013**, *52*, 847–858. [CrossRef]
41. Michalek, M.; Aisenbrey, C.; Bechinger, B. Investigation of membrane penetration depth and interactions of the amino-terminal domain of huntingtin: Refined analysis by tryptophan fluorescence measurement. *Eur. Biophys. J. Biophy.* **2014**, *43*, 347–360. [CrossRef] [PubMed]
42. Cote, S.; Wei, G.H.; Mousseau, N. Atomistic mechanisms of huntingtin N-terminal fragment insertion on a phospholipid bilayer revealed by molecular dynamics simulations. *Proteins* **2014**, *82*, 1409–1427. [CrossRef] [PubMed]
43. Ceccon, A.; Schmidt, T.; Tugarinov, V.; Kotler, S.A.; Schwieters, C.D.; Clore, G.M. Interaction of Huntingtin Exon-1 Peptides with Lipid-Based Micellar Nanoparticles Probed by Solution NMR and Q-Band Pulsed EPR. *J. Am. Chem. Soc.* **2018**, *140*, 6199–6202. [CrossRef] [PubMed]
44. Karanji, A.K.; Beasley, M.; Sharif, D.; Ranjbaran, A.; Legleiter, J.; Valentine, S.J. Investigating the interactions of the first 17 amino acid residues of Huntingtin with lipid vesicles using mass spectrometry and molecular dynamics. *J. Mass Spectrom.* **2020**, *55*, e4470. [CrossRef]
45. Goksu, E.I.; Vanegas, J.M.; Blanchette, C.D.; Lin, W.C.; Longo, M.L. AFM for structure and dynamics of biomembranes. *BBA Biomembr.* **2009**, *1788*, 254–266. [CrossRef] [PubMed]
46. El Kirat, K.; Morandat, S.; Dufrêne, Y.F. Nanoscale analysis of supported lipid bilayers using atomic force microscopy. *BBA Biomembr.* **2010**, *1798*, 750–765. [CrossRef]
47. Picas, L.; Milhiet, P.E.; Hernández-Borrell, J. Atomic force microscopy: A versatile tool to probe the physical and chemical properties of supported membranes at the nanoscale. *Chem. Phys. Lipids* **2012**, *165*, 845–860. [CrossRef]
48. Mescola, A.; Ragazzini, G.; Facci, P.; Alessandrini, A. The potential of AFM in studying the role of the nanoscale amphipathic nature of (lipo)-peptides interacting with lipid bilayers. *Nanotechnology* **2022**, *33*, 432001. [CrossRef]
49. Burke, K.A.; Godbey, J.; Legleiter, J. Assessing mutant huntingtin fragment and polyglutamine aggregation by atomic force microscopy. *Methods* **2011**, *53*, 275–284. [CrossRef]
50. Burke, K.A.; Hensal, K.M.; Umbaugh, C.S.; Chaibva, M.; Legleiter, J. Huntingtin disrupts lipid bilayers in a polyQ-length dependent manner. *BBA Biomembr.* **2013**, *1828*, 1953–1961. [CrossRef]
51. Burke, K.A.; Yates, E.A.; Legleiter, J. Biophysical insights into how surfaces, including lipid membranes, modulate protein aggregation related to neurodegeneration. *Front. Neurol.* **2013**, *4*, 17. [CrossRef] [PubMed]
52. Chaibva, M.; Burke, K.A.; Legleiter, J. Curvature Enhances Binding and Aggregation of Huntingtin at Lipid Membranes. *Biochemistry* **2014**, *53*, 2355–2365. [CrossRef] [PubMed]
53. Ho, C.S.; Khadka, N.K.; She, F.; Cai, J.; Pan, J. Polyglutamine aggregates impair lipid membrane integrity and enhance lipid membrane rigidity. *Biochim. Biophys. Acta* **2016**, *1858*, 661–670. [CrossRef] [PubMed]
54. Garcia-Manyes, S.; Sanz, F. Nanomechanics of lipid bilayers by force spectroscopy with AFM: A perspective. *BBA Biomembr.* **2010**, *1798*, 741–749. [CrossRef] [PubMed]
55. Pan, J.J.; Khadka, N.K. Kinetic Defects Induced by Melittin in Model Lipid Membranes: A Solution Atomic Force Microscopy Study. *J. Phys. Chem. B* **2016**, *120*, 4625–4634. [CrossRef]
56. Pan, J.J.; Dalzini, A.; Song, L.K. Cholesterol and phosphatidylethanolamine lipids exert opposite effects on membrane modulations caused by the M2 amphipathic helix. *BBA Biomembr.* **2019**, *1861*, 201–209. [CrossRef]
57. Aryal, C.M.; Bui, N.N.; Song, L.K.; Pan, J.J. The N-terminal helices of amphiphysin and endophilin have different capabilities of membrane remodeling. *BBA Biomembr.* **2022**, *1864*, 183907. [CrossRef]
58. Aryal, C.M.; Bui, N.N.; Khadka, N.K.; Song, L.K.; Pan, J.J. The helix 0 of endophilin modifies membrane material properties and induces local curvature. *BBA Biomembr.* **2020**, *1862*, 183397. [CrossRef]
59. Khadka, N.K.; Aryal, C.M.; Pan, J.J. Lipopolysaccharide-Dependent Membrane Permeation and Lipid Clustering Caused by Cyclic Lipopeptide Colistin. *ACS Omega* **2018**, *3*, 17828–17834. [CrossRef]
60. Adegbuyiro, A.; Sedighi, F.; Jain, P.; Pinti, M.V.; Siriwardhana, C.; Hollander, J.M.; Legleiter, J. Mitochondrial membranes modify mutant huntingtin aggregation. *BBA Biomembr.* **2021**, *1863*, 183663. [CrossRef]
61. Beasley, M.; Groover, S.; Valentine, S.J.; Legleiter, J. Lipid headgroups alter huntingtin aggregation on membranes. *BBA Biomembr.* **2021**, *1863*, 183497. [CrossRef] [PubMed]
62. Stetter, F.W.S.; Hugel, T. The Nanomechanical Properties of Lipid Membranes are Significantly Influenced by the Presence of Ethanol. *Biophys. J.* **2013**, *104*, 1049–1055. [CrossRef] [PubMed]
63. Valenza, M.; Cattaneo, E. Emerging roles for cholesterol in Huntington's disease. *Trends Neurosci.* **2011**, *34*, 474–486. [CrossRef]
64. Karasinska, J.M.; Hayden, M.R. Cholesterol metabolism in Huntington disease. *Nat. Rev. Neurol.* **2011**, *7*, 561–572. [CrossRef] [PubMed]
65. Leoni, V.; Caccia, C. The impairment of cholesterol metabolism in Huntington disease. *BBA Mol. Cell Biol. Lipids* **2015**, *1851*, 1095–1105. [CrossRef]

66. Gao, X.; Campbell, W.A.; Chaibva, M.; Jain, P.; Leslie, A.E.; Frey, S.L.; Legleiter, J. Cholesterol Modifies Huntingtin Binding to, Disruption of, and Aggregation on Lipid Membranes. *Biochemistry* **2016**, *55*, 92–102. [CrossRef]
67. Veatch, S.L.; Polozov, I.V.; Gawrisch, K.; Keller, S.L. Liquid domains in vesicles investigated by NMR and fluorescence microscopy. *Biophys. J.* **2004**, *86*, 2910–2922. [CrossRef]
68. Róg, T.; Pasenkiewicz-Gierula, M.; Vattulainen, I.; Karttunen, M. Ordering effects of cholesterol and its analogues. *BBA Biomembr.* **2009**, *1788*, 97–121. [CrossRef]
69. Pan, J.J.; Tristram-Nagle, S.; Nagle, J.F. Effect of cholesterol on structural and mechanical properties of membranes depends on lipid chain saturation. *Phys. Rev. E* **2009**, *80*, 021931. [CrossRef]
70. Brown, D.A.; London, E. Functions of lipid rafts in biological membranes. *Annu. Rev. Cell Dev. Biol.* **1998**, *14*, 111–136. [CrossRef]
71. Kollmitzer, B.; Heftberger, P.; Rappolt, M.; Pabst, G. Monolayer spontaneous curvature of raft-forming membrane lipids. *Soft Matter* **2013**, *9*, 10877–10884. [CrossRef] [PubMed]
72. Khadka, N.K.; Teng, P.; Cai, J.F.; Pan, J.J. Modulation of lipid membrane structural and mechanical properties by a peptidomimetic derived from reduced amide scaffold. *BBA Biomembr.* **2017**, *1859*, 734–744. [CrossRef] [PubMed]
73. Han, X.J.; Achalkumar, A.S.; Cheetham, M.R.; Connell, S.D.A.; Johnson, B.R.G.; Bushby, R.J.; Evans, S.D. A Self-assembly Route for Double Bilayer Lipid Membrane Formation. *Chemphyschem* **2010**, *11*, 569–574. [CrossRef]
74. Nagle, J.F.; Zhang, R.T.; TristramNagle, S.; Sun, W.J.; Petrache, H.I.; Suter, R.M. X-ray structure determination of fully hydrated L(alpha) phase dipalmitoylphosphatidylcholine bilayers. *Biophys. J.* **1996**, *70*, 1419–1431. [CrossRef] [PubMed]
75. Quinn, P.J.; Wolf, C. An X-ray diffraction study of model membrane raft structures. *FEBS J.* **2010**, *277*, 4685–4698. [CrossRef]
76. Yang, S.T.; Kreutzberger, A.J.B.; Lee, J.; Kiessling, V.; Tamm, L.K. The role of cholesterol in membrane fusion. *Chem. Phys. Lipids* **2016**, *199*, 136–143. [CrossRef]
77. Parente, R.A.; Nir, S.; Szoka, F.C. Ph-Dependent Fusion of Phosphatidylcholine Small Vesicles—Induction by a Synthetic Amphipathic Peptide. *J. Biol. Chem.* **1988**, *263*, 4724–4730. [CrossRef]
78. Murata, M.; Takahashi, S.; Kagiwada, S.; Suzuki, A.; Ohnishi, S. Ph-Dependent Membrane-Fusion and Vesiculation of Phospholipid Large Unilamellar Vesicles Induced by Amphiphilic Anionic and Cationic Peptides. *Biochemistry* **1992**, *31*, 1986–1992. [CrossRef]
79. Martens, S.; McMahon, H.T. Mechanisms of membrane fusion: Disparate players and common principles. *Nat. Rev. Mol. Cell Bio* **2008**, *9*, 543–556. [CrossRef]
80. Kabelka, I.; Pachler, M.; Prevost, S.; Letofsky-Papst, I.; Lohner, K.; Pabst, G.; Vacha, R. Magainin 2 and PGLa in Bacterial Membrane Mimics II: Membrane Fusion and Sponge Phase Formation. *Biophys. J.* **2020**, *118*, 612–623. [CrossRef]
81. Kabelka, I.; Georgiev, V.; Marx, L.; Pajtinka, P.; Lohner, K.; Pabst, G.; Dimova, R.; Vacha, R. Magainin 2 and PGLa in bacterial membrane mimics III: Membrane fusion and disruption. *Biophys. J.* **2022**, *121*, 852–861. [CrossRef] [PubMed]
82. Suopanki, J.; Götz, C.; Lutsch, G.; Schiller, J.; Harjes, P.; Herrmann, A.; Wanker, E.E. Interaction of huntingtin fragments with brain membranes—Clues to early dysfunction in Huntington's disease. *J Neurochem* **2006**, *96*, 870–884. [CrossRef] [PubMed]
83. Reddy, P.H.; Shirendeb, U.P. Mutant huntingtin, abnormal mitochondrial dynamics, defective axonal transport of mitochondria, and selective synaptic degeneration in Huntington's disease. *BBA Mol. Basis Dis.* **2012**, *1822*, 101–110. [CrossRef] [PubMed]
84. Reddy, P.H.; Mao, P.Z.; Manczak, M. Mitochondrial structural and functional dynamics in Huntington's disease. *Brain Res. Rev.* **2009**, *61*, 33–48. [CrossRef]
85. Oliveira, J.M.A. Nature and cause of mitochondrial dysfunction in Huntington's disease: Focusing on huntingtin and the striatum. *J. Neurochem.* **2010**, *114*, 1–12. [CrossRef]
86. Damiano, M.; Galvan, L.; Deglon, N.; Brouillet, E. Mitochondria in Huntington's disease. *BBA Mol. Basis Dis.* **2010**, *1802*, 52–61. [CrossRef]
87. Bossy-Wetzel, E.; Petrilli, A.; Knott, A.B. Mutant huntingtin and mitochondrial dysfunction. *Trends Neurosci.* **2008**, *31*, 609–616. [CrossRef]
88. Chen, H.C.; Chan, D.C. Mitochondrial dynamics-fusion, fission, movement, and mitophagy-in neurodegenerative diseases. *Hum. Mol. Genet.* **2009**, *18*, R169–R176. [CrossRef]
89. Shirendeb, U.; Reddy, A.P.; Manczak, M.; Calkins, M.J.; Mao, P.Z.; Tagle, D.A.; Reddy, P.H. Abnormal mitochondrial dynamics, mitochondrial loss and mutant huntingtin oligomers in Huntington's disease: Implications for selective neuronal damage. *Hum. Mol. Genet.* **2011**, *20*, 1438–1455. [CrossRef]
90. Knott, A.B.; Perkins, G.; Schwarzenbacher, R.; Bossy-Wetzel, E. Mitochondrial fragmentation in neurodegeneration. *Nat. Rev. Neurosci.* **2008**, *9*, 505–518. [CrossRef]
91. Kim, J.; Moody, J.P.; Edgerly, C.K.; Bordiuk, O.L.; Cormier, K.; Smith, K.; Beal, M.F.; Ferrante, R.J. Mitochondrial loss, dysfunction and altered dynamics in Huntington's disease. *Hum. Mol. Genet.* **2010**, *19*, 3919–3935. [CrossRef] [PubMed]
92. Khadka, N.K.; Ho, C.S.; Pan, J.J. Macroscopic and Nanoscopic Heterogeneous Structures in a Three-Component Lipid Bilayer Mixtures Determined by Atomic Force Microscopy. *Langmuir* **2015**, *31*, 12417–12425. [CrossRef] [PubMed]

93. Ho, C.S.; Khadka, N.K.; Pan, J. Sub-ten-nanometer heterogeneity of solid supported lipid membranes determined by solution atomic force microscopy. *BBA Biomembr.* **2015**, *1858*, 181–188. [CrossRef] [PubMed]
94. Pan, J.J.; Sahoo, P.K.; Dalzini, A.; Hayati, Z.; Aryal, C.M.; Teng, P.; Cai, J.F.; Gutierrez, H.R.; Song, L.K. Membrane Disruption Mechanism of a Prion Peptide (106–126) Investigated by Atomic Force Microscopy, Raman and Electron Paramagnetic Resonance Spectroscopy. *J. Phys. Chem. B* **2017**, *121*, 5058–5071. [CrossRef] [PubMed]